Local Buckling influence on the moment redistribution for continuous composite beams in bridges

Samy Guezouli, Mohammed Hjiaj, Quang Huy Nguyen

▶ **To cite this version:**

Samy Guezouli, Mohammed Hjiaj, Quang Huy Nguyen. Local Buckling influence on the moment redistribution for continuous composite beams in bridges. The Baltic Journal of Road and Bridge Engineering (BJRBE), 2010, 5 (4), pp.207-217. 10.3846/bjrbe.2010.29 . hal-00966793

HAL Id: hal-00966793
https://hal.science/hal-00966793

Submitted on 28 Mar 2014

HAL is a multi-disciplinary open access archive for the deposit and dissemination of scientific research documents, whether they are published or not. The documents may come from teaching and research institutions in France or abroad, or from public or private research centers.

L'archive ouverte pluridisciplinaire **HAL**, est destinée au dépôt et à la diffusion de documents scientifiques de niveau recherche, publiés ou non, émanant des établissements d'enseignement et de recherche français ou étrangers, des laboratoires publics ou privés.

LOCAL BUCKLING INFLUENCE ON THE MOMENT REDISTRIBUTION PERCENTAGES FOR COMPOSITE CONTINUOUS BEAMS OF BRIDGES

Samy Guezouli[1], Mohammed Hjiaj[2], Nguyen Quang Huy[3]

National Institute of Applied Sciences INSA, 20 Av. des Buttes de Coësmes 35043, Rennes, France
E-mails: [1]samy.guezouli@insa-rennes.fr, [2]mohammed.hjiaj@insa-rennes.fr,
[3]quang-.huy.nguyen@ens.insa-rennes.fr

Abstract. The present paper is concerned with the elastic design optimisation of continuous composite beams. This optimisation is based on the analysis of the beam in the inelastic range including the concrete creep and shrinkage, the tension stiffening and temperature difference effects as well as the possible local buckling instability. The finite element program "Pontmixte" (adapted to study continuous beams at real scale with short time computation) is first presented with its different sections: Pre-design (in accordance with Eurocode specifications), Non linear finite element (FE) calculation and Post-processing. In order to valid the proposed model, the numerical results are compared to experimental test ones on the example of a twin-span beam in reduced scale (7.5m length for each span) without taking into account the local buckling phenomenon avoided in the experimental test by using web-stiffeners. After that, special attention is paid to study the influence of the local buckling instability on the moment redistribution percentages from hogging to sagging zones. The application concerns different 3-span beams of bridge at real scale with medium span lengths (40m - 60m - 40m). The post-buckling behaviour represented by moment-rotation curves (M-θ) is obtained by the simulation of a simplified 3D model using Castem FE code. The hyperbolic decreasing of these curves is computed in "Pontmixte" using a specific tortional spring FE in order to take into account the local buckling phenomenon. The influence of this instability on the moment redistribution percentages calls the Eurocode predictions into question.

Keywords: Eurocodes, bridges, FEM, composite beams, local buckling, moment redistribution.

1. Introduction

Steel-concrete composite structures are common practice today in bridges and industrial buildings. The advantages of both materials lead to a very economic alternative especially in terms of high bearing capacity. The Structural Laboratory of INSA, Rennes, France set some experimental tests including one of a twin-span beam that will be used to valid the finite element model "Pontmixte" (Guezouli, Yabuki 2006). Depending on the hogging cross-section class, the Eurocodes give the max moment redistribution percentages allowed in the case of cracked or uncracked elastic global analyses, so the knowledge about the influence of some phenomena in the inelastic range on the proposed values can reduce high rectification costs. The focus is on the relative less resistant classes of cross-sections that require an Elastic Global Analysis (EGA). The local buckling begins generally before reaching the elastic bending resistance for class 4 and between elastic and plastic resistances for class 3. Experimental and finite element studies on the local buckling of steel girders have been described in many papers (Skaloud, Rokey 1972; Davies, Mandal 1979; Shanmugam, Wan Mohtar 2007) and the elastic as well as the inelastic behaviour of plate girders having uniform cross-section along the beam is well understood. Without taking into account a specific classification of these cross sections, Skaloud and Rokey (1972) concluded that the ultimate load carrying capacity is influenced by the flexural rigidity of the flanges for girders having similar proportions to those employed in civil engineering construction and Porter *et al.* (1975) assumed that the failure will occur when a certain region of the web yields as a result of the combined effect of the inclined tensile membrane stress field and the web buckling stress. So, it appears that the combined rigidity of compressed flange and the web, for a steel panel under negative bending moment, remains the first parameter influencing the load carrying capacity of the cross-section..

2. The model "Pontmixte"

Fig. 1 shows the main organisation of "Pontmixte" with its different options. The program has its graphical post-processor "Pmixtpost" for plotting needed variable all along the beam or against the increasing load (Guezouli, Aribert 2001). The continuous beam could be pre-designed with constant cross-section along the beam (for buildings) or different flange thicknesses on hogging zone than those in sagging zone (for bridges) (Brozzetti 2000; CEN 2004). The algorithm select the most critical loading cases on hogging and sagging zones between the possible ones (example: for a twin-span beam, 4 possible loading cases for asymmetrical beams reduced to 2 cases for symmetrical ones if both distributed and concentrated variable loads could be applied to the beam). In the case of class 3 or 4 cross-sections on hogging zone, the unknown values of bottom flange thicknesses could be found by an iterative process balanced between two critical loading cases:

- critical loading case in sagging zone: maximum moment close to the plastic resistant moment;
- critical loading case on hogging zone: maximum moment close to the elastic resistant moment.

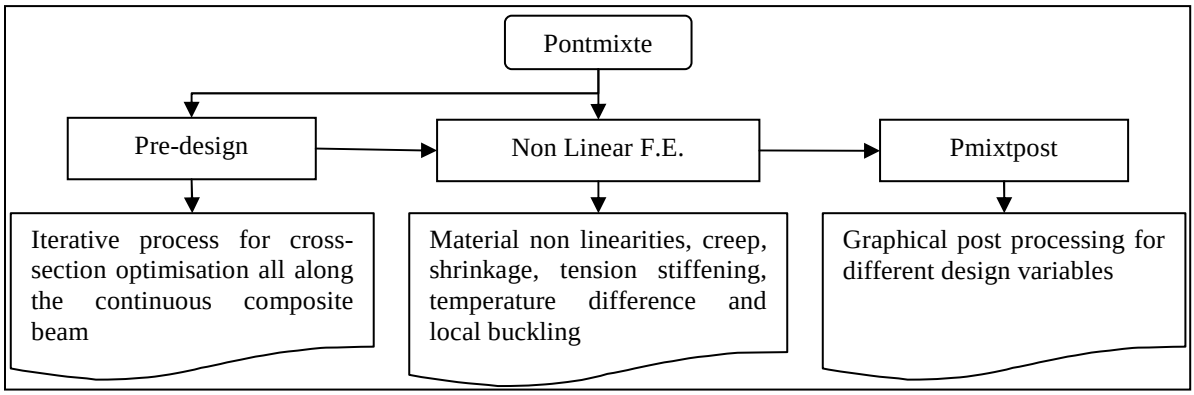

Fig. 1. Main organisation of "Pontmixte"

Different finite element analyses of composite beams have been carried out (Guezouli, Aribert 2001; Chung, Sotelino, 2006; Nguyen, Hjiaj, Uy, Guezouli 2008). The finite element model (Fig. 2) concerned with the program "Pontmixte considers a concrete slab with reinforcing steels connected to a steel girder. The composite beam finite element (node i to node j) has 4 degrees of freedom per node:

$$\{d_e\} = \left\{u_i^{(c)} \quad u_i^{(a)} \quad v_i \quad \theta_i \quad u_j^{(c)} \quad u_j^{(a)} \quad v_j \quad \theta_j\right\}^t \quad (1)$$

For the node "i" for example (Fig. 2), the longitudinal displacements are: $u_i^{(c)}$ for the concrete slab and $u_i^{(a)}$ for the steel girder applied at each corresponding centre of gravity, the vertical displacement v_i and the rotation θ_i both applied at the neutral axis of the entire composite cross-section. The stud slip is defined by:

$$\gamma_i = u_i^{(c)} - u_i^{(a)} + d \times \theta_i \quad (2)$$

where d is the distance between the slab and the girder neutral axis.

First numerical integration is performed along the element (2 Gauss points) and the second one concerns each fibre constituting the entire composite cross-section (Fig. 3). Non linear equations are solved using a step-by-step method including a secant algorithm (Fig. 4). The automatic longitudinal mesh of the beam could be in accordance with the connection distribution or not. Along the beam, 5 Gauss points are necessary in the variable part of the beam (slope = 1/4) and 2 Gauss points are enough elsewhere.

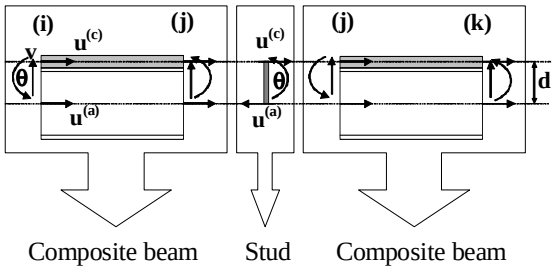

Fig. 2. Composite beam finite element

The calculation remains running until the imposed stopping calculation (such as reaching the elastic moment at intermediate support, or application of the whole defined loads etc.). This generally occurs before anyone of the following material failure criteria is reached:

- max compression in the concrete slab;
- max strain in the steel girder;
- max strain in the reinforcing steel;
- max slip of the stud.

The convergence of the iterative process is tested on the norm of the displacements limited to 10^{-4}.

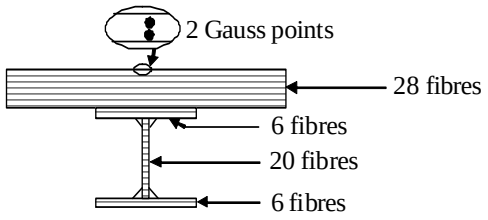

Fig. 3. Cross-section integration

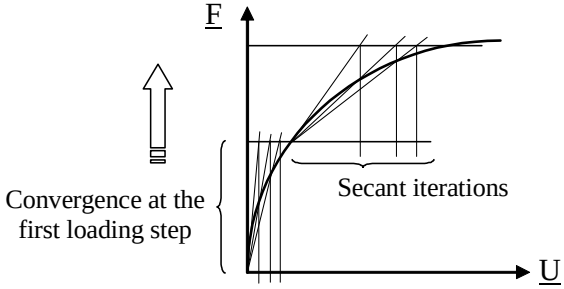

Fig. 4. Step-by step with secant algorithm

The symmetrical stiffness matrix of the composite beam element (*ij*) including a stud at the node "j" for example, is presented in Eq (3) with the following notation:

$k_{ij}^{(c)}$: the *ij* value in the concrete stiffness matrix (6×6);

$k_{ij}^{(a)}$: the *ij* value in the girder stiffness matrix (6×6);

R_{ij}: the *ij* value in the stud stiffness matrix (3×3).

The specific finite element for local buckling instability (Fig. 5) includes longitudinal displacements for the concrete slab and the girder connected to a tortional spring. The (Moment-Rotation) curve of the local buckling will be followed as soon as the point (M_v, θ_v) is

reached. This point represents the beginning of the buckling and will be numerically established.

The secant stiffness of the buckling finite element can be easily added at appropriate degrees of freedom in Eq (3).

$$[K]=\begin{bmatrix} k_{11}^{(c)} & 0 & k_{12}^{(c)} & k_{13}^{(c)} & k_{14}^{(c)} & 0 & k_{15}^{(c)} & k_{16}^{(c)} \\ & k_{11}^{(a)} & k_{12}^{(a)} & k_{13}^{(a)} & 0 & k_{15}^{(a)} & k_{16}^{(a)} & k_{16}^{(a)} \\ & & \left(k_{22}^{(c)}+k_{22}^{(a)}\right) & \left(k_{23}^{(c)}+k_{23}^{(a)}\right) & k_{24}^{(c)} & k_{24}^{(a)} & \left(k_{25}^{(c)}+k_{25}^{(a)}\right) & \left(k_{26}^{(c)}+k_{26}^{(a)}\right) \\ & & & \left(k_{33}^{(c)}+k_{33}^{(a)}\right) & k_{34}^{(c)} & k_{34}^{(a)} & \left(k_{35}^{(c)}+k_{35}^{(a)}\right) & \left(k_{36}^{(c)}+k_{36}^{(a)}\right) \\ & & & & \left(k_{44}^{(c)}+R_{11}\right) & R_{12} & k_{45}^{(c)} & \left(k_{46}^{(c)}+R_{13}\right) \\ & & & & & \left(k_{44}^{(a)}+R_{22}\right) & k_{45}^{(a)} & \left(k_{46}^{(a)}+R_{23}\right) \\ & & & & & & \left(k_{55}^{(c)}+k_{55}^{(a)}\right) & \left(k_{56}^{(c)}+k_{56}^{(a)}\right) \\ \textit{Sym.} & & & & & & & \left(k_{66}^{(c)}+k_{66}^{(a)}+R_{33}\right) \end{bmatrix} \quad (3)$$

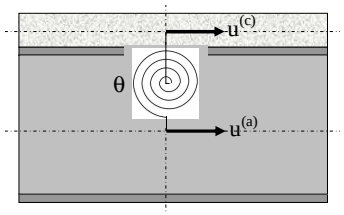

Fig. 5. Local buckling element with tortional spring

3. Material behaviours

Material behaviour curves are shown on Fig. 6 using following Eqs:

$$\underline{\text{Concrete}}:\ \frac{\sigma^{(c)}}{f_{cm}}=\frac{k\eta-\eta^2}{1+(k-2)\eta} \quad (4)$$

with: $\eta=\dfrac{\varepsilon^{(c)}}{\varepsilon_m}>0$ and $k=1.1E_{cm}\dfrac{\varepsilon_m}{f_{cm}}$

$$\underline{\text{Stud}}:\ Q=Q_u\left(1-e^{-c_1|\gamma|}\right)^{c_2} \quad (5)$$

The parameters c_1 and c_2 (Eq (5)) depend on the ductility of the stud and can be easily obtained using a push-out test; usual values are: c_1 = 0.7 and c_2 = 0.8. In order to take into account the creep effect (Fig. 6d), the elastic modulus of the concrete is reduced to $E^{(c)}=E^{(a)}/n_\phi$, where $E^{(a)}$ is the usual elastic modulus of structural steel and n_ϕ is the modular ratio (for first steps loading: n_ϕ = ∞, when the concrete slab is dry: n_ϕ = 18 and leads to: n_ϕ = 6).

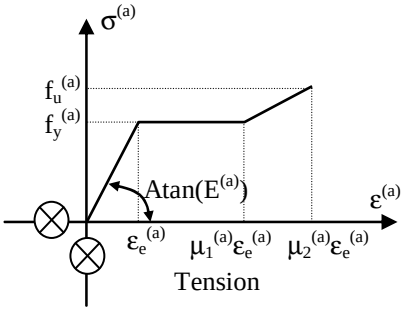

Fig. 6a. Steel girder behaviour

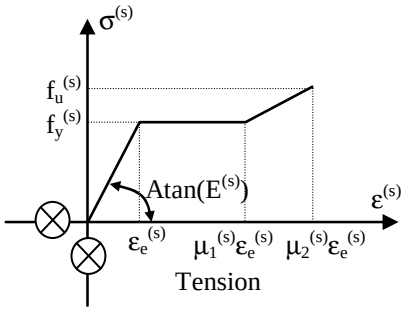

Fig. 6b. Reinforcing steel behaviour

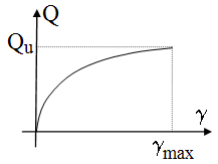

(2)

Fig. 6c. Ductile stud behaviour

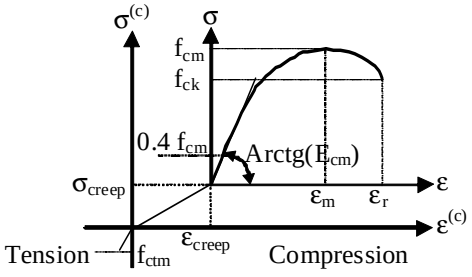

Fig. 6d. Concrete behaviour with creep

The temperature difference effect is considered by a superposition of a tension N_{sh} in the concrete slab and a compression in the neutral axis of the composite cross-section (homogenised with n_ϕ = 12, Fig. 7) with: $N_{sh}=\varepsilon_{sh}^{\infty}A^{(c)}E^{(a)}/n_\phi$ and $M_{sh}=N_{sh}\times x_{sh}$. If the temperature difference between slab and steel girder is about ±5 °C, the total shrinkage including the temperature effect for usual concrete can vary from $\varepsilon_{sh}^{\infty}=3.5\times10^{-4}$ (dry environment) to $\varepsilon_{sh}^{\infty}=2.5\times10^{-4}$ (most favourable environment).

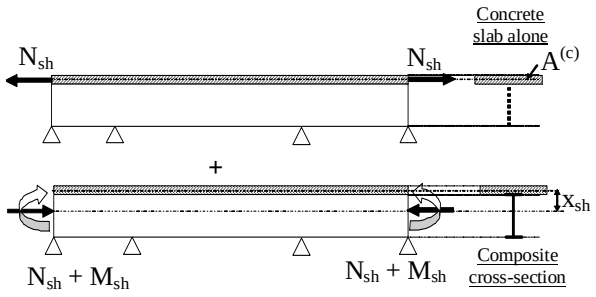

Fig. 7 Temperature and shrinkage effect

The tension stiffening effect (Fig. 8a) is limited between two lines:

- uncracked stage (concrete and reinforcing steel resisting together):

$$F^{(s,\varepsilon_1)} = E^{(s)}A^{(s)}(1+n\rho)\varepsilon_1\,, \qquad (6)$$

with: $n = \dfrac{E^{(s)}}{E^{(c)}}$ and $\rho = \dfrac{A_t^{(c)}}{A^{(s)}}$ ($A_t^{(c)}$ the area of the slab in tension);

- full cracked stage (reinforcing steel resisting alone):

$$F^{(s,\varepsilon_2)} = E^{(s)}A^{(s)}\varepsilon_2\,. \qquad (7)$$

Between both precedent limits, the tension stiffening is acting since the beginning of the concrete cracking corresponding to a stress equal to f_{ctm} (Fig. 8b). Contrary to the homogenization in steel equivalence of the reinforced slab in tension used to obtain the Eq (6), the homogenization must be done now in concrete equivalence to obtain the limit of the uncracked stage $\varepsilon_{1,max}$ corresponding to f_{ctm}.

$$\varepsilon_{1,max} = \frac{f_{ctm}}{E^{(c)}(1+n^{-1}\rho^{-1})} \qquad (8)$$

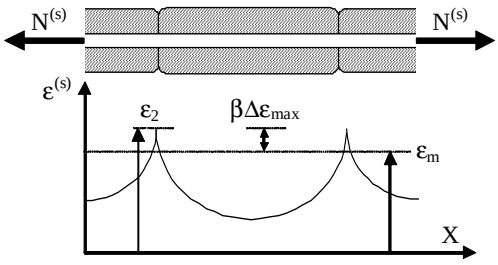

Fig. 8a. Tension stiffening phenomenon

If $F^{(s,\varepsilon_1)} > F^{(s,\varepsilon_{1,max})}$, the average strain corresponding to the tension stiffening effect is defined with the following relationship : $\varepsilon_m = \varepsilon_2 - \beta\Delta\varepsilon_{max}$, where $\beta\Delta\varepsilon_{max}$ represents the part due to the concrete between cracks with the parameter β = 0.4 for high adherence bars. Using a hyperbolic model for $\Delta\varepsilon_{max}$ and considering the Eqs (6) – (7), ε_m becomes:

$$\varepsilon_m = \frac{F^{(s,\varepsilon_2)}}{E^{(s)}A^{(s)}} - \beta\frac{F^{(s,\varepsilon_2)}}{F^{(s,\varepsilon_m)}} = \frac{F^{(s,\varepsilon_2)}}{E^{(s)}A^{(s)}} - \beta\frac{F^{(s,\varepsilon_2)}}{F^{(s,\varepsilon_m)}} \times \frac{F^{(s,\varepsilon_{1,max})}}{E^{(s)}A^{(s)}(1+n\rho)}$$

$$\Leftrightarrow \quad \varepsilon_m = \frac{F^{(s,\varepsilon_2)}}{E^{(s)}A^{(s)}}\left[1-\beta\frac{F^{(s,\varepsilon_{1,max})}}{(1+n\rho)F^{(s,\varepsilon_m)}}\right] \qquad (9)$$

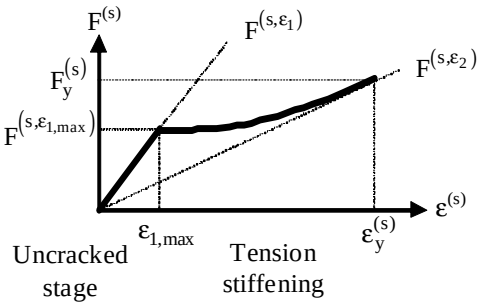

Fig. 8b. Tension stiffening model

4. FE model validation

The pre-design algorithm leads for the twin-beam under investigation (Fig. 9) to a hogging cross-section of class 3. In sagging zones, the cross-section is assumed to be of classe 1 because the slab is fully connected to the girder. An uncracked elastic global analysis is used with the following material mechanical characteristics:

- concrete slab Young's modulus: $E^{(c)}$ = 36000 MPa;
- steel girder Young's modulus: $E^{(a)}$ = 190000 MPa;
- reinforcing steel Young's modulus: $E^{(s)}$ = 200000 MPa.

The self weight is taken into account (4.17 kN/m for sagging zones and 4.26 kN/m for hogging ones). Only concentrated loads are applied on the beam, a load P applied at the left mid-span increases proportionally to a load Q applied at the right mid-span.

- For the first critical loading case (the one concerning the sagging zone), only P is applied,
- For the second critical loading case (the one concerning the hogging zone), both P and Q are applied proportionally.

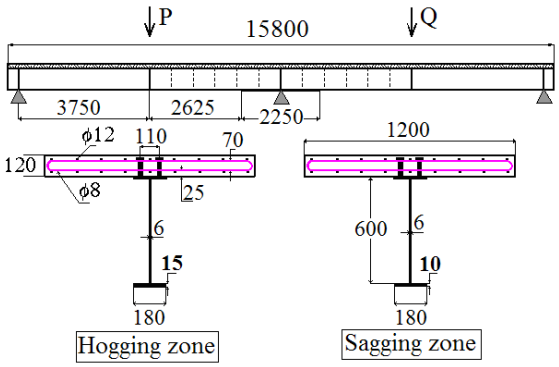

Fig. 9. Geometrical characteristics of the twin-beam

It is assumed that the hogging zone concerns 15% of the span length on each side of the intermediate support. For this zone, the pre-design algorithm proposes 15 mm for the bottom flange thickness while for other cross-sections in sagging zones only 10 mm are required. The top flange thickness is equal to the bottom one. After the beam pre-design, a non linear calculation is carried out with the following loading history: the load P applied at the left mid-span increases proportion-

ally to the load Q applied at the right mid-span until 550 N. At this load level, Q remains constant and P still increases until reaching one of the failure criteria described above. Mechanical characteristics are summarised in Table 1. Figs. 10 and 11 respectively, show that the comparison between numerical and experimental results is satisfactory both for deflexion (unfortunately the measurements under the load Q have not been done), and for the bending moment under the load P at the intermediate support. Numerical and experimental failures are reached by concrete cracking under the load P for P + Q ≈ 1400 kN giving:

- maximum displacement under P:

$w_{\max}^{exprimental} = 48mm$; $w_{\max}^{numerical} = 45mm$

- maximum moment at intermediate support:

$M_{\max}^{-experimental} = 960kNm$; $M_{\max}^{-numerical} = 963kNm$

- maximum moment (kNm) under P:

$M_{\max}^{+experimental} = 1140kNm$; $M_{\max}^{+numerical} = 1130kNm$

It is noted that the real conditions of the specimen test where considered in this numerical simulation taking into account the tension stiffening, the concrete creep and shrinkage as well as the temperature difference effect. Without these options, the results could not be as close as those obtained.

This validation does not include the local buckling phenomenon because the concrete cracking (max compression) occurred before as the failure criterion. For this reason, the simulation of a continuous beam at real scale with hogging cross-sections of class 3 or 4 appears necessary to simulate the local buckling using the specific finite element defined in Fig. 5.

Table 1. Mechanical characteristics

Material	Parameters values
Concrete slab	E_{cm} = 36 000 MPa, f_{ck} = 40 MPa, f_{cm} = 48 MPa, f_t = 2 MPa, ε_m = 0.0022, $\varepsilon_r^{(c)}$ = 0.004
Steel girder	$E^{(a)}$ = 190 000 MPa, $f_y^{(a)}$ = 475 MPa, $f_u^{(a)}$ = 620 MPa, $\mu_1^{(a)}$ = 10, $\mu_2^{(a)}$ = 28
Reinforcing steel	$E^{(s)}$ = 200 000 MPa, $f_y^{(s)}$ = 443 MPa, $f_u^{(s)}$ = 565 MPa, $\mu_1^{(s)}$ = 1, $\mu_2^{(s)}$ = 32, $\varepsilon_u^{(s)} = \mu_2^{(s)} \varepsilon_e^{(s)}$
Stud	Q_u = 80 000 N, c_1 = 0.7, c_2 = 0.8, γ_{max} = 6 mm

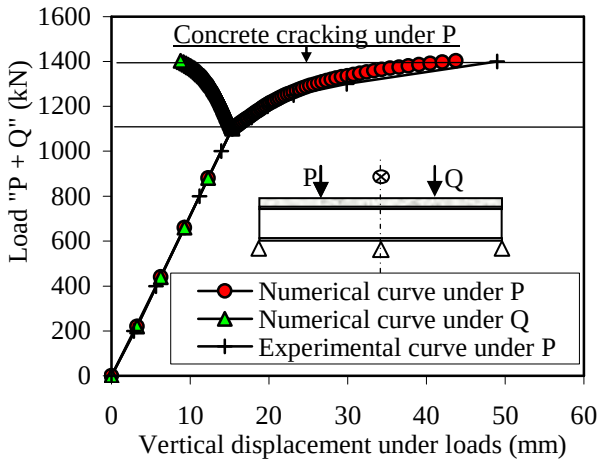

Fig. 10 Comparison of deflexions

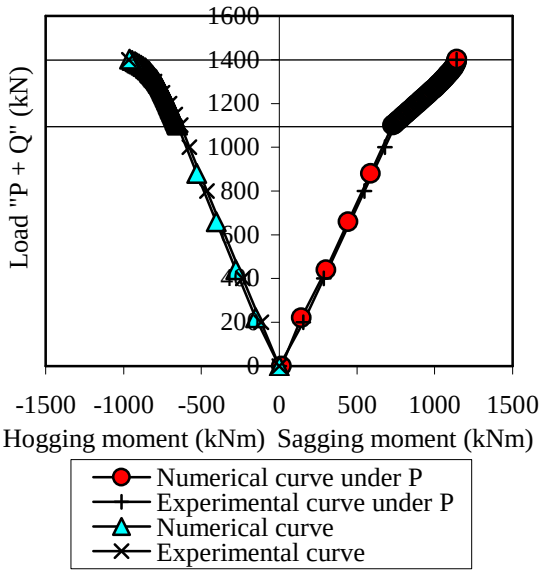

Fig. 11. Comparison of bending moments

5. Influence of local buckling on the moment redistribution for a continuous beam at real scale

Firstly, the pre-design of the 3-span beam leads to a hogging cross-section of class 3 and a bottom flange as well as the web of class 3 (Fig. 13). Mechanical characteristics are given in Table 2.

Table 2. Mechanical characteristics

Material	Parameters values
Concrete slab	E_{cm} = 35 000 MPa, f_{ck} = 40 MPa, f_{cm} = 48 MPa, f_t = 3.5 MPa, ε_m = 0.0025, $\varepsilon_r^{(c)}$ = 0.0035
Steel girder	$E^{(a)}$ = 210 000 MPa, $f_y^{(a)}$ = 355 MPa, $f_u^{(a)}$ = 510 MPa, $\mu_1^{(a)}$ = 10, $\mu_2^{(a)}$ = 25
Reinforcing steel	$E^{(s)}$ = 200 000 MPa, $f_y^{(s)}$ = 400 MPa, $f_u^{(s)}$ = 432 MPa, $\mu_1^{(s)}$ = 1, $\mu_2^{(s)}$ = 25
Stud	Q_u = 174 900 N, c_1 = 0.7, c_2 = 0.8, γ_{max} = 6 mm

For reminder, the whole cross-section class is the max one between the compressed flange and the web. Table 3 shows different cross-sections provided for by this investigation taking care to be always in the case of a girder cross-section of class 3. The cross-section obtained by the pre-design is noted H5, it represents the less resistant one by comparison to the other ones (H1 to H4) for which the thicknesses were arbitrarily increased or decreased in order to vary the classes of the bottom flange and the web from class 1 to 3. It should be noted that the flange thicknesses in sagging zones remain the same for all the beams, the web thickness is constant all along each beam, the selfweight of the girder becomes different from one beam to another and the critical position of concentrated variable loads Q is the same for all the beam in the case of type A (symmetrical loading case) and supposed the same in the case of type B (asymmetrical loading case). It is pointed out that only the pre-designed beam remains optimized at ULS and SLS. Geometrical characteristics of hogging cross-

sections are given in Table 4 with also some arbitrary modifications proposed for the web and the bottom flange giving always a girder cross-section of class 4 on hogging. The traffic loads applied to the bridge (here a twin-steel girder bridge) have values in accordance with the Model 1 of EN 1991-2 Part 2, namely a "U.D.L." of 9 kN/m^2 for the lane 1 and 2.5 kN/m^2 for the lanes 2 and 3, and a Tandem System with 2 axle loads each equal to 300 kN. In the transverse direction the traffic loads are distributed according to a linear influence line. Finally, the numerical characteristic values of traffic loads for the most loaded lane are: q = 31.2 kN/m and Q1 = Q2 = 406 kN (with the distance 1200 mm).

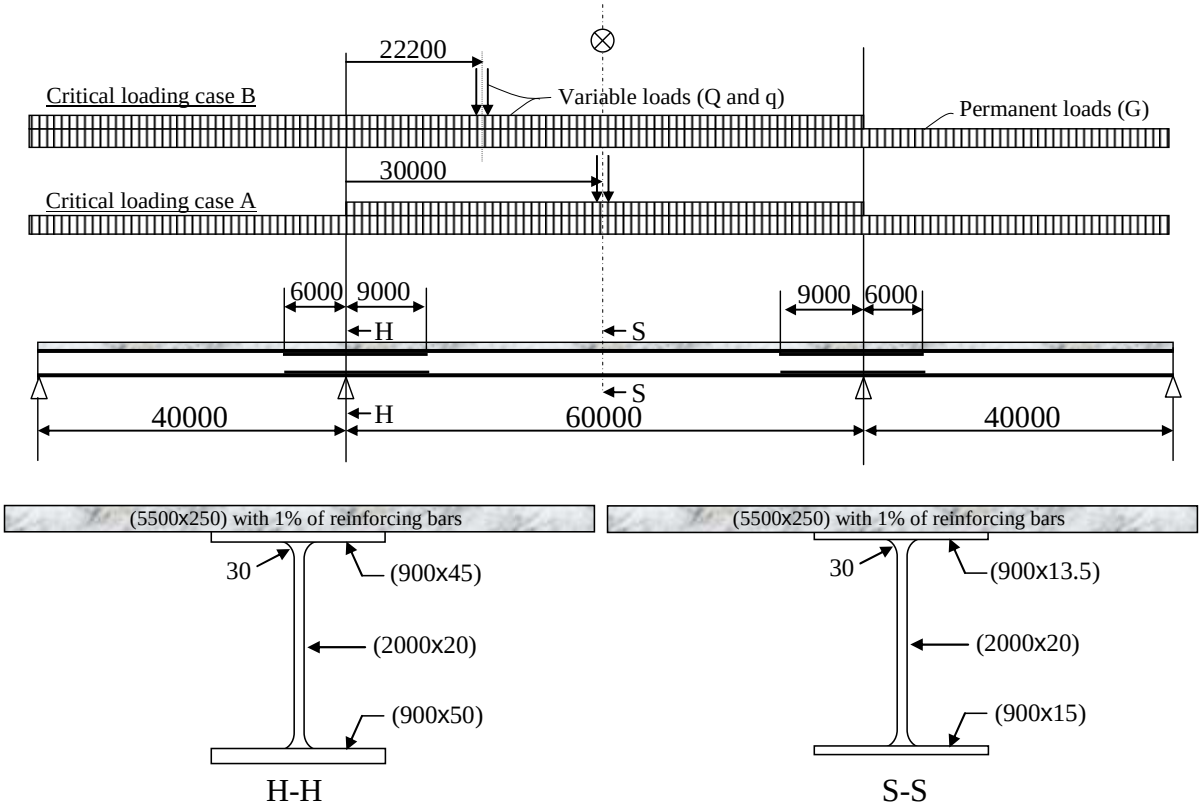

Fig. 12. Pre-design results and critical loading cases

Table 3. Cross-sections under investigation on hogging zone – Class 3

Cross-section	Web thickness, mm	Web Class	Bottom flange thickness, mm	Bottom flange class	Cross-section class
H1	30	1	50	3	
H2	25	2	50	3	
H3	20	3	60	1	3
H4	20	3	55	2	
H5	20	3	50	3	

Table 4. Cross-sections under investigation on hogging zone – Class 4

Cross-section	Web thickness, mm	Web Class	Bottom flange thickness, mm	Bottom flange class	Cross-section class
K1	30	1	35	4	
K2	25	2	35	4	
K3	20	3	35	4	
K4	15	4	60	1	4
K5	15	4	55	2	
K6	15	4	50	3	
K7	15	4	35	4	

5.1. A 3-D FE model for buckling curves (M-θ)

The 3-D model developed on Cast3M (2003) (Fig. 13) represents the steel girder as well as the stiffeners meshed by 4-nodes shells, the studs are meshed using 3D beams to ensure the displacements continuity with the shells (same degrees of freedom) and the reinforcing bars are replaced by equivalent shells supposed at the top of the studs. The panel length is equal to twice the web height (h_w) beginning from the cross-section H-H.

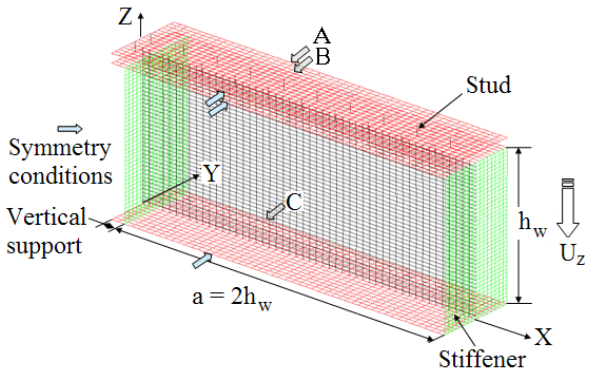

A and B (top flange and bars):
For all the nodes along X axis: $U_{yy} = 0$
If same conditions for C (bottom flange):
(M-θ) curve concerns only local buckling otherwise it may includes also the lateral tortional buckling

Fig. 13. Simplified 3-D model

It is supposed that on hogging zone the concrete slab is totally cracked so it does not need to be modellized. Nevertheless, very stiff springs should be modellized to keep same distance between the top flange of the girder and the reinforcing bars during the loading. It's pointed out that the springs have no influence on the shear behavior of the studs (Faella, Martinelli, Nigro 2002; Guezouli, Hjiaj, Nguyen 2008). This simplification requires common mesh nodes between the studs and the reinforcing bars. The comparison of the transverse displacements of the web at ultimate limit state (Figs 14a, 14b) shows clearly that the addition of very stiff spring elements to the model has a negligible influence on the mechanical behaviour and the studs appear working exclusively in shear. The model is loaded by applying a displacement at its end to avoid possible geometrical element distortion. The vertical displacement *Uz* equal to 200 mm is applied in 10 steps.

The curves (M-θ) are plotted for different cross-sections of class 3 (Fig. 15) and of class 4 (Fig. 16). The rotation capacity of the cross-section is similar for all the cross-sections. The max point of each curve represents the beginning of the local buckling (M_v, θ_v). After this point, a hyperbolic decreasing model (Eq (10)) could be adopted with appropriate values for M_0, M_v and θ_v (M_0 represents a horizontal asymptotic line). The web thickness has a largest influence on these curves than the bottom flange one (on the initial stiffness and also on the max hogging moment). The decreasing curves after buckling is similar with nearly the same value of buckling rotation ($\theta_v \approx 0.014$ rad). The curve related to Eq (10) plotted for H1 as an example, gives a good prediction for the behaviour after buckling. The buckling rotation is also nearly the same in the case of cross-section of class 4 ($\theta_v \approx 0.012$ rad).

$$M = M_0 + (M_v - M_0)\frac{\theta_v}{\theta}, \quad \forall \theta \geq \theta_v \qquad (10)$$

Remarks:

- Before setting about a non-linear stability calculation, a linear stability one is carried out and the whole displacement field is reduced by a scale of 1/20 in the aim to represent an initial deformation of the specimen.
- There is no significant sense to talk about available rotation capacity at the intermediate support for cross-sections of classes 3 and 4 because of the local buckling instability.

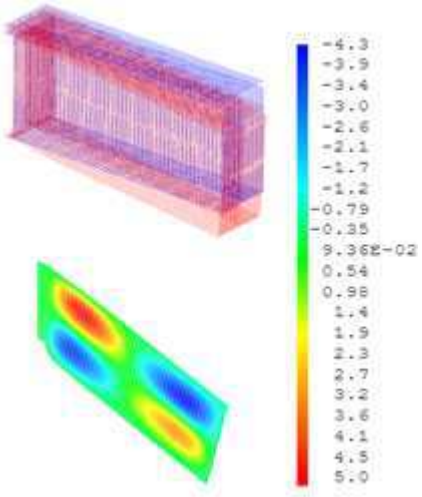

Fig. 14a. Without springs

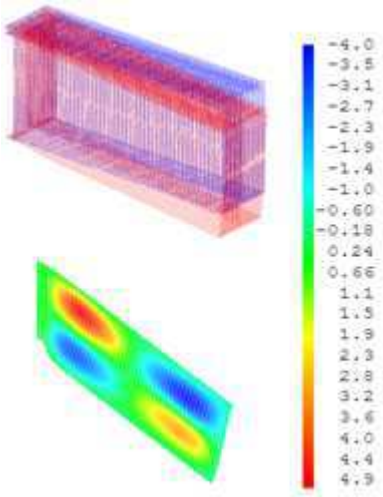

Fig. 14b. With springs

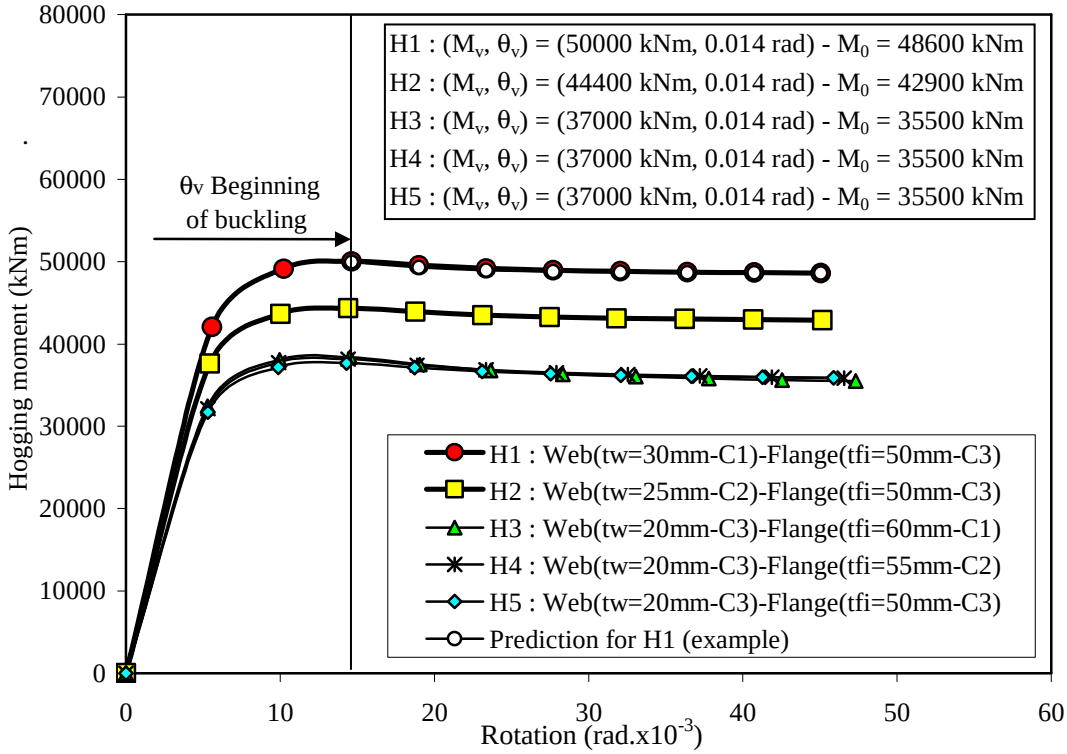

Fig. 15. 3-D calculations and buckling curves – Class 3

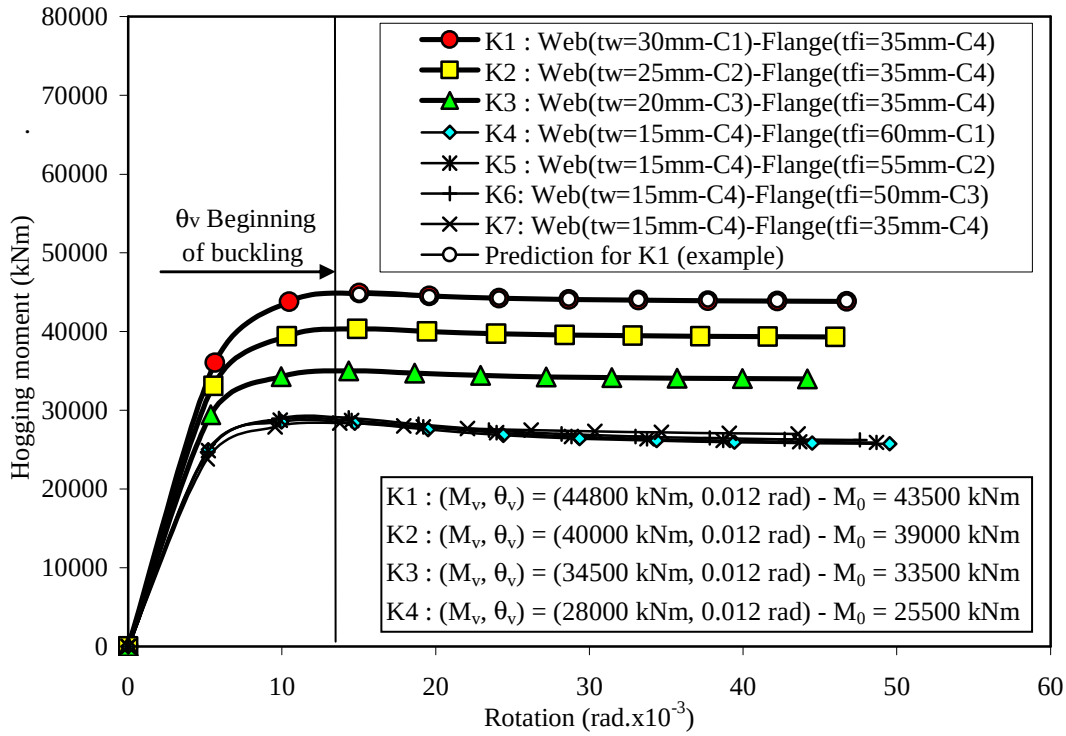

Fig. 16. 3-D calculations and buckling curves – Class 4

5.2. The results

The moment redistribution percentage is calculated with the following Eq:

$$R = \frac{\left|M_{Ed.Rd}^{-(uncr)} - M_{1+2}^{-}\right| - \left|M_{el.Rd}^{-(num)} - M_{1+2}^{-}\right|}{\left|M_{Ed.Rd}^{-(uncr)} - M_{1+2}^{-}\right|} \times 100 \qquad (11)$$

where $M_{el.Rd}^{-(num)}$ – the numerical hogging moment obtained for H-H cross-section; $M_{Ed.Rd}^{-(uncr)}$ – the hogging moment obtained by a virtual elastic calculation (using the same loading level λ); M_{1+2}^{-} – the hogging moment resulting only from the first and second loading steps corresponding respectively to the selfweight of the girder and the one of the concrete that is still

wet (Guezouli, Aribert 2004; Guezouli 2007; Guezouli, Yabuki 2008). During these steps, the cross-section is not considered resisting as a composite cross-section so, this part of bending moment must be subtracted to the ones defined previously. The proposed hyperbolic model is computed in the user friendly program "Pontmixte" and different applications are carried out with appropriate values of the model parameters (M_0, M_v and θ_v). The stopping calculation criterion is either reaching the plastic resistant moment in sagging zone (generally occurs for the critical loading case of type A) or the elastic moment resistant at the intermediate support (generally occurs for the critical loading case of type B).

5.2.1. Results for the beams of class 3

Different variables concerned with the Eq (11) without and with taking into account possible local buckling are given respectively in Tables 5, 6. The variation of the hogging moment against the cumulative load (Figs 17, 18, 19), show that:

- for the beams H1 and H2, the elastic resistant moment is reached before the buckling characteristic point (M_v, θ_v): no influence of local buckling on the moment redistribution percentage, the cross-sections seams to be relatively resistant;
- for the beams H3, H4 and H5, without taking into account the local buckling, the rule of 10% redistribution predicted in the Eurocodes seams to be questionable especially for loading case of type A but the occurrence of local buckling decreases the value of the numerical hogging moment increasing consequently the value of the redistribution R. This value becomes finally over than 10% for both loading cases. Because of local buckling, the calculation stops for lower values of λ ($\lambda^{\text{buckling}} \leq \lambda^{\text{no buckling}}$) especially for loading case of type B and necessary the elastic moment $M_{\text{Ed.Rd}}^{-(\text{uncr})}$ changes and the value of R consequently. In the column of λ (Tables 4, 5), the letters correspond to the stopping calculation criterion for each beam [(A) $\rightarrow M_{pl.Rd}^{+}$ and (B) $\rightarrow M_{el.Rd}^{-}$].

Table 5. Hogging and sagging bending (kNm) – Related to Table 3 (class 3)

All options – Local buckling not included

Beams	$M_{\text{el.Rd}}^{-(\text{num})}$	$M_{\text{Ed.Rd}}^{-(\text{uncr})}$	M_{1+2}^{-}	$M_{\text{pl.Rd}}^{-}$	$M_{\text{Sd}}^{+(\text{num})}$	$M_{\text{pl.Rd}}^{+}$	λ	R, %
Loading case of type A (for reminder see Fig. 13)								
H1	– 41706	– 43653	– 17232	– 48958	37058	37563	1.71(B)	7
H2	– 39825	– 41166	– 16987	– 47072	33374	33541	1.51(A)	6
H3	– 37698	– 39046	– 17090	– 51843	29228	29462	1.35(A)	6
H4	– 37632	– 38712	– 16927	– 48487	29285	29462	1.35(A)	5
H5	– 37556	– 38340	– 16745	– 45150	29350	29462	1.35(A)	4
Loading case of type B (for reminder see Fig. 13)								
H1	– 41722	– 47264	– 17232	– 48958	32472	37563	1.54(B)	18
H2	– 40529	– 45027	– 16987	– 47072	29742	33541	1.40(B)	16
H3	– 45685	– 49123	– 17090	– 51843	28872	29462	1.60(B)	11
H4	– 42460	– 45793	– 16927	– 48487	27625	29462	1.42(B)	11
H5	– 39969	– 43146	– 16745	– 45150	26948	29462	1.35(B)	12

Table 6. Hogging and sagging bending (kNm) – Related to Table 3 (class 3)

All options – Local buckling included

Beams	$M_{\text{el.Rd}}^{-(\text{num})}$	$M_{\text{Ed.Rd}}^{-(\text{uncr})}$	M_{1+2}^{-}	$M_{\text{pl.Rd}}^{-}$	$M_{\text{Sd}}^{+(\text{num})}$	$M_{\text{pl.Rd}}^{+}$	λ	R, %
Loading case of type A (for reminder see Fig. 13)								
H1	– 41706	– 43653	– 17232	– 48958	37058	37563	1.71(A)	7
H2	– 39825	– 41166	– 16987	– 47072	33374	33541	1.51(A)	6
H3	– 36379	– 39046	– 17090	– 51843	29229	29462	1.35(A)	12
H4	– 36371	– 38712	– 16927	– 48487	29285	29462	1.35(A)	11
H5	– 36362	– 38340	– 16745	– 45150	29350	29462	1.35(A)	9
Loading case of type B (for reminder see Fig. 13)								
H1	– 41722	– 47264	– 17232	– 48958	32472	37563	1.54(B)	18
H2	– 40529	– 45027	– 16987	– 47072	29742	33541	1.40(B)	16
H3	– 36220	– 46051	– 17090	– 51843	28074	29462	1.41(B)	34
H4	– 36578	– 44832	– 16927	– 48487	27335	29462	1.36(B)	29
H5	– 36746	– 43146	– 16745	– 45150	26995	29462	1.35(B)	24

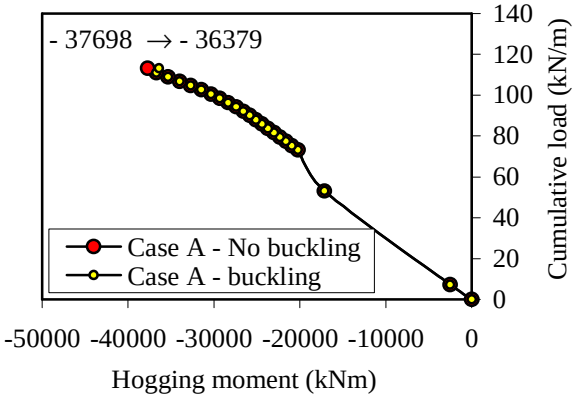

Fig. 17a. (θ – M) – Case A – Beam H3

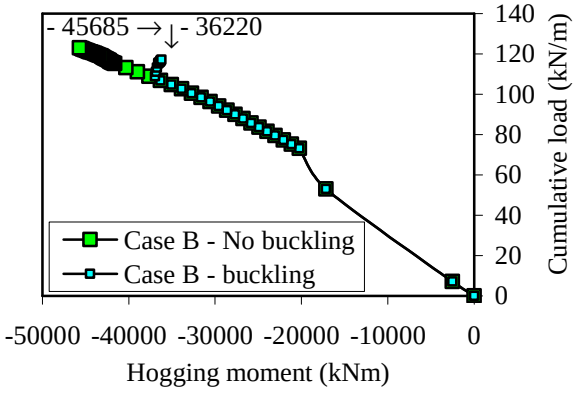

Fig. 17b. (θ – M) – Case B – Beam H3

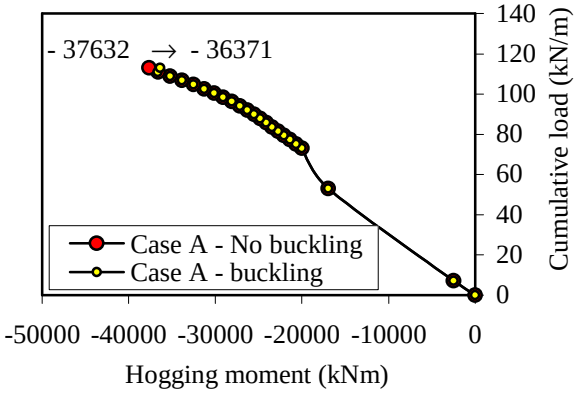

Fig. 18a. (θ – M) – Case A – Beam H4

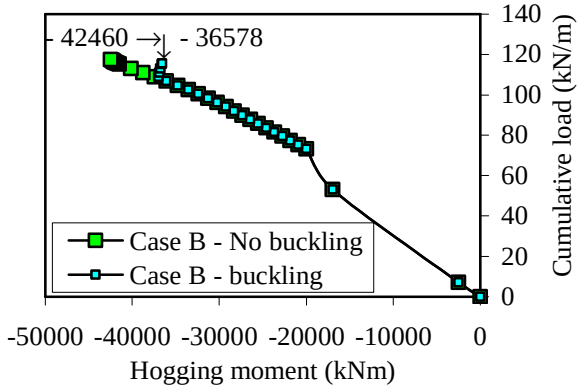

Fig. 18b. (θ – M) – Case B – Beam H4

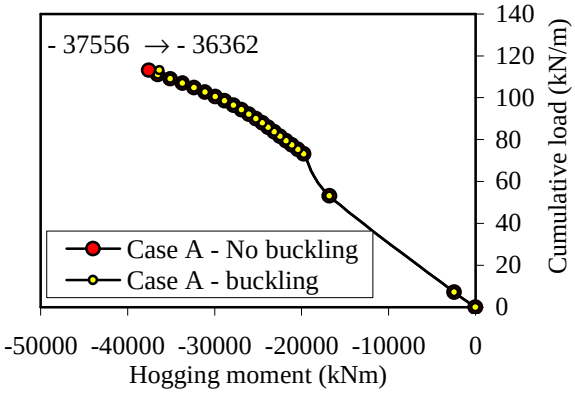

Fig. 19a. (θ – M) – Case A – Beam H5

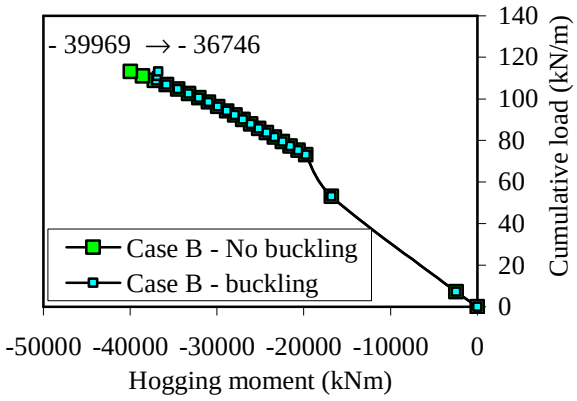

Fig. 19b. (θ – M) – Case B – Beam H5

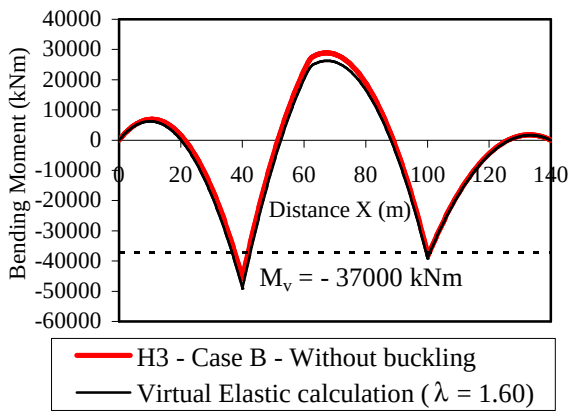

Fig. 20a. H3 case B without buckling

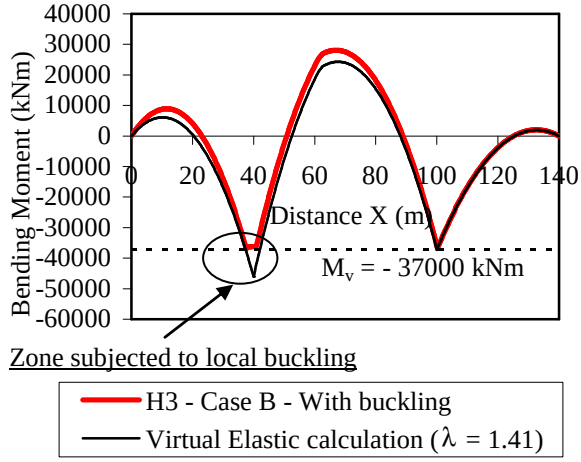

Fig. 20b. H3 case B with buckling

Table 7. Hogging and sagging bending – Related to Table 4 (class 4)

All options – Local buckling not included

Beams	K1	K2	K3	K4	K5	K6	K7
Loading case of type A (for reminder see Fig. 13)							
λ	1.35(B)	1.22(B)	1.01(B)	1.22(A)	1.15(A)	1.15(A)	0.81(B)
R, %	24	19	16	2	1	– 0.0	12
Loading case of type B (for reminder see Fig. 13)							
λ	1.15(B)	1.01(B)	0.88(B)	1.46(B)	1.35(B)	1.15(B)	0.74(B)
R, %	30	28	25	7	8	9	21

Table 8. Hogging and sagging bending (kNm) – Related to Table 4 (class 4)

All options – Local buckling included

Beams	K1	K2	K3	K4	K5	K6	K7
Loading case of type A (for reminder see Fig. 13)							
λ	1.35(B)	1.22(B)	1.01(B)	1.15(A)	1.15(A)	1.15(A)	0.81(B)
R, %	24	19	16	53	52	50	20
Loading case of type B (for reminder see Fig. 13)							
λ	1.15(B)	1.01(B)	0.88(B)	1.35(B)	1.22(B)	1.08(B)	0.74(B)
R, %	30	28	25	67	61	55	29

It must be noted that the beams H1 and H4 have been arbitrary defined on hogging zone stronger than the one obtained by the pre-design optimization (H5); this leads necessary to values of $\lambda \geq 1.35$. For example, the loading case B of the beam H3, the numerical bending moment can be plotted along the beam by comparison to the virtual elastic calculation. Without local buckling (Fig. 20a) the elastic hogging bending is obtained while the lower layer of the girder bottom flange reaches its elastic limit (this occurs for $\lambda = 1.60$, value which the curves are plotted for). It is clear that for this critical loading case, the left intermediate support is mostly concerned with the local buckling than the right one (see the dot-line corresponding to buckling moment). If the local buckling is taken into account (Fig. 20b), the same stopping calculation criterion than the one described before is obtained for a lower loading level ($\lambda = 1.41$). First finite element begins to buckle on the left intermediate support in accordance with the corresponding buckling model and the equilibrium of the forces along the beam must be carried out. The local buckling is extended on both sides defining the zone subjected to this instability.

5.2.2. Results for the beams of class 4

In the case of class 4, Tables 7, 8 summarize only the values of the moment redistribution percentages. Eq (11) has to be calculated with moments under loads corresponding to the specific value of λ. These values are generally less than 1.35 because most of the beams are less resistant than the pre-designed one. The local buckling appears also more sensible for loading case of type B than the one of type A. Very low values of R especially for the loading case A are increasing when the local buckling is taken into account. Sometimes could be negative meaning that the redistribution is inverted and happens from mid-spans to intermediate supports. The influence of local buckling on the moment redistribution percentage appears more important in the case of class 4 than in the case of class 3.

6. Conclusions

This study attempted to show that it is possible to simulate at a real scale the behaviour in the inelastic range of a steel-concrete composite bridge beam with a relative simple finite element formulation. The comparison of numerical and experimental results in the case of a twin-span beam in reduced scale (1/2) ensures the validation of the proposed model. After that, the main interest concerned the beams with cross-sections of class 3 and 4 on hogging zone that are generally subjected to the local buckling instability. A prior study was concerned with the post-buckling behaviour of a 3D panel on hogging zone to obtain the moment-rotation relationship corresponding to these cross-section classes. A hyperbolic model was proposed depending on 3 parameters: the buckling point (M_v, θ_v) and the horizontal asymptotic line $M = M_0$. This model was computed in the code "Pontmixte" and several numerical simulations were carried out to show the significant influence of the local buckling instability on the moment redistribution percentage from hogging to sagging zones in the case of a 3-span beam bridge at real scale. This influence appears closely linked to the class combination of the compressed flange and the web of the girder. The local buckling mostly occurs when the web is of a higher class (less resistant) than the compressed flange. In this case, if the local buckling is not taken into account, the rule of 10% moment redistribution proposed by the Eurocodes is questionable especially for the loading case of type A. If the local buckling is taken into account, the calculation of the moment redistribution percentage after buckling until elastic resistant moment is given only for information and it must not be included in the elastic design because specific constructive measures (web-stiffeners) are required to avoid the local buckling instability and consequently assures the possibility of this redistribution. Skaloud and Zörnerova (2005) paid attention to the post-buckled behaviour and ultimate strength of slender webs; similar approach could be carried out for steel-concrete composite beams

and easily computed in the code "Pontmixte". This future prospect could give important information about the influence of the "breathing" web on the moment redistribution percentage.

References

Guezouli, S.; Yabuki, T. 2006. "Pontmixte": a user friendly program for continuous beams of composite bridges, *International Colloquium on Stability and Ductility of Steel Structures, SDSS'06*, Lisbon, Portugal.

Skaloud, M.; Rokey, K. C. 1972. The ultimate load behaviour of plate girders loaded in shear, *Journal of Structural Engineering* 50(1): 29–47.

Davies, G.; Mandal, S. N. 1979. The collapse behavior of tapered plate girders loaded within the tip, *Ice Proceedings* 67(1): 65–80. DOI**:** 10.1680/iicep, 2317.

Shanmugam, N. E.; Wan Mohtar, W. H. M. 2007. Experimental and finite element studies on tapered steel plate girders, in *Proc of the 3rd International Conference on Steel and Composite Structures (ICSCS-2007)*, Manchester, UK, pp. 165–170.

Porter, D. M.; Rokey, K. C.; Evans, H. R. 1975. The collapse behavior of plate girders loaded in shear, *Journal of Structural Engineering* 53(8): 313–325.

Guezouli, S.; Aribert, J. M. 2001. Approche aux éléments finis pour l'étude du comportement des poutres de ponts mixtes à l'échelle réelle. *XVème Congrès Français de Mécanique*, Nancy, 3-7 septembre 2001. France.

Brozzetti, J. 2000, Design development of steel-concrete composite bridges during construction. Journal of Constructional Steel Research, 63: 475-84.

CEN (European Committee for Standardisation), prEN 2003 – Part 2. *Design of composite steel and concrete structures – Rules for bridges*. Stage 34 draft revised, Brussels.

Nguyen, Q.H.; Hjiaj, M.; Uy, B. and Guezouli, S. 2008, Nonlinear F.E. analysis of composite beams, *Eurosteel 2008*, Gratz, Austria.

Chung W.; Sotelino, 2006. E.D. Three-dimensional finite element modeling of composite girder bridges. *Engineering Structures* 28 63-71.

Cast3M, 2003. Un code de calcul pour l'analyse de structures par la méthode des éléments finis (E.F) et la modélisation en mécanique des fluides. CEA, Sarclay

Faella, C.; Martinelli, E. and Nigro, E. 2002. Steel and concrete beams with flexible shear connection: Exact analytical expression of the stiffness matrix and applications. *Computers and Structures* 80: 1001-9.

Guezouli, S.; Hjiaj, M. and Nguyen, Q.H. 2008, 3-D F.E. Connection degree in composite continuous beams – Influence on the bending moment capacity, *Eurosteel 2008*, Gratz, Austria.

Guezouli, S.; Aribert, J. M. 2004. Numerical Investigation of moment redistribution in continuous beams of composite bridges, in *Proc of the 5th International Conference "Composite Construction in Steel and Concrete V"*. Ed. by Leon, T. R.; Lange, J. Kruger National Park, South Africa. American Society of Civil Engineers, 47–56. DOI : 10.1061/40826(186)5.

Guezouli, S. 2007. Local buckling of class 4 cross-section – application to a steel-concrete continuous beam of bridge at real scale, in *Proc of the 3rd International Conference on Steel and Composite Structures (ICSCS-2007.)* Manchester, UK, p. 481–487.

Guezouli, S. and Yabuki, T. 2008, Numerical Investigation on instabilities of steel-concrete composite cross-sections, *5th International Conference on Thin-Walled Structures ICTWS08*, Brisbane, Australia.

Skaloud M. and Zörnerova M. 2005. Fatigue behavior of the breathing webs of steel bridge girders, *Journal of Civil Engineering and Management Vol XI, N° 4, 323-336.*

Received 12 February 2009; accepted